Kinetics of Oxygen Adsorption and Initial Oxidation on Cu(110) by Hyperthermal Oxygen Molecular Beams†

Kousuke Moritani,*,‡ Michio Okada,§,||,⊥ Yuden Teraoka,‡ Akitaka Yoshigoe,‡ and Toshio Kasai||

Synchrotron Radiation Research Center, Japan Atomic Energy Agency, 1-1-1 Kouto, Sayo, Hyogo 679-5148, Japan, Renovation Center of Instruments for Science Education and Technology, Osaka University, 1-2 Machikaneyama-cho, Toyonaka, Osaka 560-0043 Japan, Department of Chemistry, Graduate School of Science, Osaka University, 1-1 Machikaneyama-cho, Toyonaka, Osaka 560-0043, Japan, and PRESTO, Japan Science and Technology Agency, 4-1-8 Honcho, Kawaguchi, Saitama, 332-0012, Japan

Received: June 14, 2009; Revised Manuscript Received: September 12, 2009

Oxygen adsorption and subsequent oxide formation on Cu(110) using a hyperthermal oxygen molecular beam (HOMB) were investigated using X-ray photoelectron spectrometry. The O-uptake curves, which were determined from the evolution of the O-1s peaks, indicate that simple Langmuir type kinetics can describe dissociative adsorption of O_2 with an incident energy (E_i) below 0.5 eV under $\Theta \leq 0.5$ ML. The reaction order dependence on E_i implies two competing dissociation mechanisms, trapping-mediated and directly activated adsorption. Oxidation at $\Theta \geq 0.5$ ML proceeds rather effectively using highly energetic HOMB at $E_i \geq 1.0$ eV. The azimuthal dependence of the sticking probability during the effective oxidation using HOMB incidence suggests that the added rows, which consist of the Cu−O structure, shade the reactive hollow sites in the trough where oxygen penetrates into the subsurface. The surface Cu_2O formed with highly energetic HOMB incidence decomposes with desorbing subsurface oxygen even at room temperature, demonstrating that HOMB can induce a metastable surface structure that cannot be produced in the thermal equilibrium process.

1. Introduction

To understand various industrially important processes, including oxide layer formation, catalytic oxidation, and corrosion, the elemental steps in the oxidation of transition metals are crucial. Among transition metals, copper is one of the common materials in practical applications, including nanoscale wiring,[1] Cu_2O-based solar-cells,[2] and oxidation catalysts.[3] Hence, numerous studies have examined oxygen adsorption and the subsequent oxidation on copper surfaces. The kinetics of oxide formation strongly depends on the crystal plane of copper because the energetic preference for the −Cu−O−Cu− chains along the [001] direction dominates oxygen incorporation. Thus, investigating the face dependent oxidation process is important for fabricating Cu_2O films in an efficient and tunable way.

The chemisorption of oxygen on Cu(110) has been investigated in numerous experimental[4−17] and theoretical[18−21] studies. Oxygen adsorbs dissociatively on Cu(110) at room temperature (RT). However, the results of low temperature scanning tunneling microscopy (STM) study have suggested the possible existence of weakly bound molecular oxygen.[4] Experimental studies using O_2 molecular beams have suggested two competing dissociation mechanism, trapping-desorption channel and directly activated dissociation channel.[5,6] Hodgson et al. have found that activated dissociative chemisorption becomes the main reaction channel for translational energies greater than ∼0.2 eV, whereas trapping-desorption dominates at translational energies below 50 meV.[5] Two theoretical studies estimated the activation barrier for dissociation to be about 0.1−0.3 eV.[18,20] The dissociative chemisorption of oxygen causes the $p(2 \times 1)$-O phase to form.[7−9] STM studies have revealed that the structure and growth mechanism of the $p(2 \times 1)$-O phase with a saturation O coverage of 0.5 ML.[10,11] Oxygen atoms are located between the topmost Cu atoms, and form a Cu−O chain along the [001] direction, which is called an added row. Cu atoms dissolve from the step edges even at RT, diffuse on terraces, and then trap oxygen adatoms. At exposures above $\sim 10^5$ L, which correspond to $\sim 10^{19}$ molecules·cm^{-2}, formation of the $c(6 \times 2)$-O phase is induced at RT.[12,13] After further oxygen exposures, Cu_2O formation has been observed on Cu(110).[14,15] However, temperatures above 480 K are required for desorbing the adsorbed oxygen.[16]

Recently, we have reported that a hyperthermal O_2 molecular beam (HOMB) induces oxidation of copper surfaces at room temperature.[22−29] In these studies, we have proposed a collision-induced absorption (CIA) mechanism for Cu_2O formation by HOMB on Cu(100)[22] and (111).[25] However, the high efficiency of oxide formation on Cu(110) suggests that the CIA process is negligible on Cu(110).[26] The oxidation process on an open Cu(110) surface seems to be more complicated than those for Cu(100) and Cu(111) substrates. The (110) facet has the [001] direction, which is favorable for forming Cu_2O because Cu−O rows form easier on the (110) facet compared to the (100) and (111) facets, and this feature is the reason Cu(110) surfaces have a rather complex oxidation mechanism. The oxidation kinetics on a Cu(410) surface indicates that a process with opening

† Part of the "Vincenzo Aquilanti Festschrift".

* To whom correspondence should be addressed. E-mail: moritani@eng.u-hyogo.ac.jp. Present address: Department of Mechanical and System Engineering, Graduate School of Engineering, University of Hyogo, 2167 Shosha, Himeji, Hyogo 671-2201.

‡ Japan Atomic Energy Agency.

§ Renovation Center of Instruments for Science Education and Technology, Osaka University.

|| Department of Chemistry, Graduate School of Science, Osaka University.

⊥ PRESTO.

10.1021/jp905564m © 2009 American Chemical Society
Published on Web 10/07/2009

pathways for subsurface migration and oxygen incorporation at high temperature is favored at (110) steps, whereas the CIA process by hyperthermal O_2 incidence occurs on (100) terraces at RT. Unraveling the face dependent oxidation mechanism is fundamentally important to more efficiently fabricate Cu_2O thin films.

Herein we investigate oxygen adsorption and subsequent oxidation processes on Cu(110) with HOMB. The O-uptake curves, which are determined from evolution of O-1s peaks, indicate that dissociative adsorption of O_2 with an incident energy (E_i) below 0.5 eV under an O coverage (Θ) below 0.5 ML follows simple Langmuir type kinetics. The reaction orders of the Langmuir equation between one and two implies two competing dissociation mechanism, trapping-mediated, which is dominant at low E_i, and directly activated adsorption, which becomes important with increasing E_i. Oxidation at $\Theta > 0.5$ ML proceeds effectively by energetic O_2 at $E_i \geq 1.0$ eV. The azimuthal dependence of the sticking probability (S) during the effective oxidation with highly energetic HOMB suggests that HOMB opens a new reaction channel via the trough of the added row where oxygen penetrates into subsurface sites. The surface Cu_2O formed by 2.3 eV HOMB decomposes by desorbing subsurface oxygen even at RT, which means that HOMB can induce a metastable surface structure that cannot be produced in the thermal equilibrium process.

2. Experimental Section

All experiments were performed with a surface reaction analysis apparatus (SUREAC 2000) constructed in BL23SU at SPring-8.[30] The surface reaction analysis chamber was equipped with an electron energy analyzer (OMICRON 5MCD) and Mg/Al Kα twin-anode X-ray source (OMICRON DAR400). A supersonic-molecular-beam apparatus, which had a differentially pumped chamber, was conjunct with the soft-X-ray synchrotron beamline. A differentially pumped quadrupole mass spectrometer, which was used to analyze the molecular species in the HOMB, was located in the line of the molecular beam axis. The base pressure of the surface reaction chamber was about 2×10^{-8} Pa. Details of the experimental apparatus are described elsewhere.[31]

The Cu(110) sample was cleaned by repeatedly sputtering with 1-keV-Ar^+ ions and annealing at 870 K until impurities were not detected by X-ray photoelectron spectrometry (XPS) with SR and the low-energy electron diffraction (LEED) showed a sharp 1×1 pattern with a low background. The O_2 molecules were dosed on the Cu(110) by backfilling O_2 gas at 1.33×10^{-5} to 1.33×10^{-4} Pa or by HOMB.

HOMB was generated by adiabatic expansion of O_2 seeded in He and/or Ar. The nozzle was composed of pyrolytic boron nitride (PBN), which is one of the most inert and heat resistant ceramic materials. The orifice diameter of the nozzle was 0.1 mm. A skimmer with a 1.0 mm diameter aperture at the top was placed 6 mm downstream from the nozzle, and a beam collimator with 5 mm diameter was attached to the surface reaction chamber. The beam diameter at the sample position was ~9 mm. The nozzle could be annealed up to 1400 K by resistive heating of the graphite ribbon heater. We verified the chemical composition of HOMB using a quadrupole mass spectrometer (QMS) and were able to exclude oxygen dissociation in the beam even at $T_n = 1400$ K because an increase in the peak at $m/z = 16$ was not detected.

Changing the seeding ratio and the nozzle temperature from RT to 1400 K controlled the kinetic energy of incident O_2. The kinetic energy was calculated from following standard equation

$$E_i = \frac{M_i}{\langle M \rangle}\left\langle \frac{\gamma}{1-\gamma} \right\rangle k_B T \quad (1)$$

where E_i and M_i are the translational energy and mass of the i-component of the gas mixture, respectively. $\langle M \rangle$ is the average mass, γ is the ratio of constant pressure and constant volume specific heat, T_n is the nozzle temperature, and k_B is Boltzmann's constant. Equation 1 is valid only for an almost perfect adiabatic expansion, that is, complete transformation of enthalpy into translational energy. Thus, we verified its validity by measuring the time-of-flight (TOF) spectrum of the direct beam using QMS. The kinetic energies were estimated from average arrival time of HOMB. For a seeded beam (0.5% O_2 in He) with $T_n =$ RT and 1400 K, the experimentally estimated upper limits were $E_i = 0.5$ and 2.3 eV, respectively, indicating a good adiabatic expansion. This result was confirmed by further checks for HOMB with different seeding ratios and $T_n = 1400$ K, leading to $0.9 \leq E_i \leq 1.5$ eV. Thus, we assumed that HOMB has a small energy dispersion generated from the adiabatic expansion, although the experimentally estimated value of the translational energy may include a relatively large error bar.

The O_2 flux at the sample position was estimated experimentally before and/or after each measurement. The estimation method is described elsewhere.[32] Briefly, we used QMS to measure the ratio (R_b) between O_2 and the inert carrier gas concentration and an ion gauge to measure the total pressure increase in the surface reaction analysis chamber (ΔP). The flux (Q_a) was then estimated from eq 2

$$Q_a = \frac{\Delta P}{A((x_a/S_a) + (x_b/S_b)R_b)}, \quad [\mathrm{Torr \cdot \mathit{l}/cm^2 \cdot s}] \quad (2)$$

where x_j and S_j are the ionization probability of the mass spectrometer and the pumping speed for particle j, respectively, and A is the beam spot area. Typical oxygen fluxes for 0.1, 0.16, 0.23, 0.35, 0.5, 1.0, and 2.3 eV HOMB were 4.7×10^{13}, 1.1×10^{14}, 1.6×10^{14}, 3×10^{14}, 3×10^{14}, 7×10^{13}, and 2×10^{14} molecules$\cdot$cm^{-2} in the normal incidence case, respectively.

The incident direction of the HOMB was along the surface normal of the sample or the oblique direction tilted 45° from the surface normal direction with the azimuthal angle direction along the high symmetry directions [$1\bar{1}0$] and [001]. The background pressure and oxygen partial pressure during the HOMB irradiation were 5×10^{-6} Pa and 1×10^{-7} Pa, respectively. After irradiation with a proper amount of HOMB, high-resolution XPS spectra were measured by a hemispherical electron energy analyzer, which was directed to the surface normal, using a monochromatic SR beam. We also observed the LEED pattern of the Cu(110) surface after measurements of XPS spectra. All experiments were performed at RT.

3. Results and Discussion

Figure 1 shows the typical evolution of the O 1s SR-XPS spectra during 2.3 eV HOMB incidence along the surface normal on a Cu(110) surface at RT. Θ was determined from the O 1s intensity by comparing Cu(100)$-(2\sqrt{2} \times \sqrt{2})$R45°$-$O ($\Theta =$ 0.5 ML) with a correction for the face-dependent Cu density. The O 1s XPS peak had a binding energy $E_B = 529.9$ eV but intensified at the same position as Θ was increased up to ~0.7 ML. A (2×1) LEED pattern corresponding to $p(2 \times 1)$-O-added row began to appear above 0.1 ML. After the (2×1) structure was fully developed at 0.5 ML, a $c(6 \times 2)$ LEED pattern started to appear and was completed at $\Theta \sim 0.7$ ML.

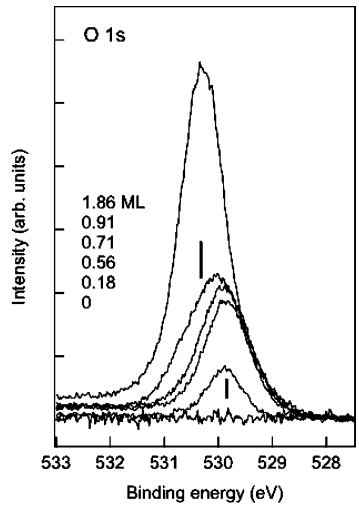

Figure 1. Evolution of O1s SR-XPS spectra for 2.3 eV HOMB incidence along the surface normal at RT.

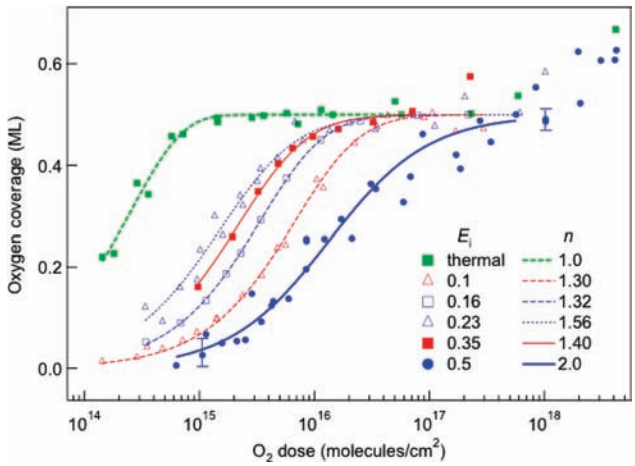

Figure 2. Uptake curves of O on Cu(110) for 0.1, 0.16, 0.23, 0.35, and 0.5 eV HOMB incidence along the surface normal and thermal O_2 dose at RT. Uptake curves are determined by integrating the O-1s XPS spectra. ML unit represents the number of atoms per surface Cu atom. Thick broken curve for thermal O_2 dose and thick solid curve for 0.5 eV HOMB incidence are fitted by a simple Langmuir model described by $d\Theta/dF = fk_{ad}(\Theta_s - \Theta)^n$ with $n = 1.0$ and 2.0, respectively. Thin solid and broken curves are the best fit curves for the respective uptake curves.

Above $\Theta > 0.7$ ML, the XPS intensity shifted slightly to 530.3 eV. The O 1s intensity at a higher binding energy and a higher coverage was assigned to the oxygen in the subsurface sites of Cu_2O.[17] In all cases, all the oxygen adsorbed dissociatively because peaks were not located above 532 eV.

Figure 2 shows the O-uptake curves for 0.1−0.5 eV HOMB generated at T_n = RT and the thermal O_2 dose. Each uptake curve was produced by integrating the O-1s XPS peaks. The HOMBs were irradiated along the surface normal direction. The intensity of the O-1s peak increased as Θ increased up to 0.5 ML, which is the tentative saturation coverage for thermal and hyperthermal O_2 with $E_i < 0.5$ eV, and a large exposure of $\sim 1 \times 10^{18}$ molecules·cm^{-2} was required to attain a coverage above 0.5 ML.

On the copper surface, an oxygen adatom causes a strong repulsive potential;[33] thus, O_2 molecules approaching the top of O-adatom should be scattered into the vacuum. Therefore, the sticking probability varies with coverage as does the probability of finding adjacent empty sites. Such adsorption processes can be described by Langmuir type kinetics. All the uptake curves under $\Theta < 0.5$ ML were well fitted by a simple Langmuir adsorption model (Figure 2). The rate equation for the adsorption of molecule is described as follows

$$d\Theta/dF = f \cdot k_{ad}(\Theta_s - \Theta)^n \quad (3)$$

where Θ, Θ_s, F, f, n, and k_{ad} are the O coverage, saturation O coverage, dose of O_2 molecules, flux density of O_2 molecules, reaction order, and adsorption-rate constant, respectively. F is proportional to the HOMB irradiation time. Because the desorption rate of oxygen adsorbed on the Cu(110) surface was negligible under $\Theta \leq 0.5$ ML at RT,[16] the desorption process did not need to be considered. In this simple Langmuir equation, the reaction orders of $n = 2$ and 1 generally corresponded to dissociative and nondissociative adsorption, respectively, because the reaction order corresponds to the number of adsorption sites required in the adsorption. Figure 2 also shows that the uptake curves for the thermal O_2 dose and 0.5 eV HOMB incidence were well reproduced by eq 3 with $n = 1.0$ and 2.0, respectively. On the other hand, those for 0.1−0.35 eV HOMB incidence were best fitted by eq 3 with a fractional reaction order of $n = 1.30-1.56$, which include error bars less than $\pm$ 0.15.

The uptake curve for thermal O_2 exposure fitted by eq 3 with $n = 1.0$ suggests a trapping-mediated adsorption mechanism where thermal O_2 molecules are trapped molecularly and then adsorbed dissociatively. An O_2 molecule impinging with a low kinetic energy is trapped on the surface in a physisorption well.[5,6,21] The O_2 molecule, which is loosely bound to the surface, diffuses across the surface and eventually dissociates at an energetically favorable site. In the trapping process for low energy O_2 molecules, the steering effect plays an important role.[33] Molecules with a low translational energy should experience steering that rotates the molecule to an energetically favorable reaction pathway. Thus, the O_2 impinges toward the unstable site, for example, the top copper atoms can be also trapped and dissociate on the surface.[20] The short-lived chemisorbed O_2 precursor that bounded weakly on the surface are also predicted.[21] The steering is possible even for chemisorbed precursor. The steering mechanism may explain the larger S value for thermal O_2 exposure than that for 0.5 eV HOMB incidence.

On the other hand, second-order kinetics ($n = 2$) of the Langmuir model well reproduced the uptake curve for 0.5 eV HOMB incidence. This is interpreted as typical dissociative adsorption requiring two adsorption sites. Liem et al. examined the dissociation of O_2 on Cu(110) at 300 K using ab initio dynamics simulations.[20] In this study, the activation barrier for O_2 dissociation on Cu(110) depends on the adsorption sites and is estimated to be 0.1−0.3 eV. Because an incident energy of 0.5 eV is sufficient to overcome the activation barrier for dissociative adsorption, directly activated chemisorptions is reasonable in the second-order kinetics for 0.5 eV HOMB. At high translational energies, the steering effect is less important due to the short collision time when passing through the interaction potential. Thus, when O_2 molecules approach the low activation barrier with sufficient energy to overcome the barrier, dissociation readily occurs once an O_2 molecule collides with the surface. On the other hand, when O_2 molecules encounter a higher activation barrier, for example, at the top of Cu atom, they scatter without dissociation.[20] Additionally, impinging O_2 molecules with a high translational energy tend

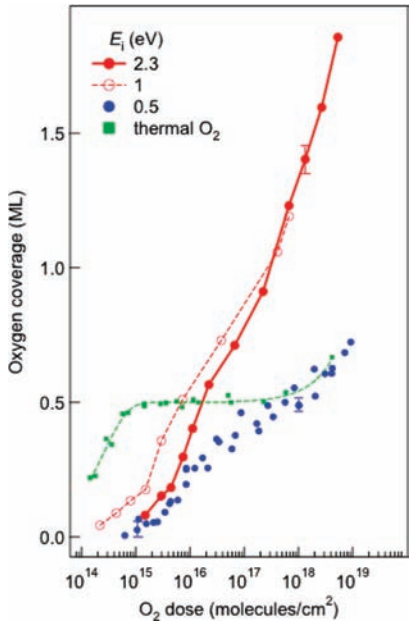

Figure 3. Uptake curves of O on Cu(110) for 0.5, 1.0, 2.3 eV HOMB incidence along the surface normal and thermal O_2 exposure at RT. Uptakes are determined by integrating the O-1s XPS spectra. ML unit represents the number of atoms per surface Cu atom.

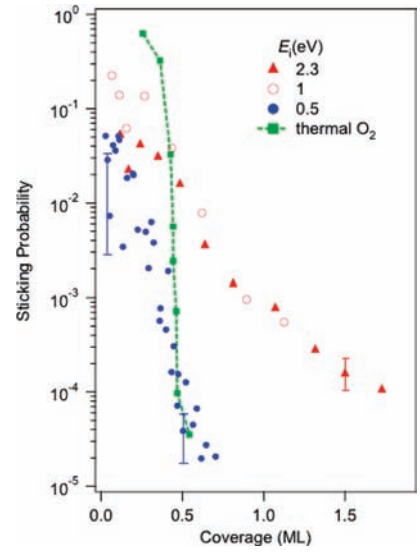

Figure 4. Coverage dependence of the sticking probability (S) on Cu(110) for 0.5, 1.0, and 2.3 eV HOMB incidence along the surface normal and thermal O_2 exposure at RT. S is calculated from the oxygen uptake curves in Figure 3.

to scatter from the surface before they dissipate their translational energy and are then trapped on the surface. Therefore, S for 0.5 eV HOMB incidence is smaller than that for thermal O_2 exposure.

The uptake curves for the HOMB with $E_i = 0.1-0.35$ eV were fitted with a fractional reaction order of $n = 1.30-1.56$ in eq 3, suggesting a combination of first and second order processes. The portion of trapping-mediated adsorption decreased with increasing translational energy of the impinging O_2 because an O_2 molecule with excess translational energy tends to scatter from surface before dissipating its energy during a collision on the surface and becomes trapped at a physisorption well. In contrast, the portion of directly activated adsorption increased because O_2 with $E_i \geq 0.1$ eV can overcome the activation barrier of 0.1−0.3 eV when it collides on a suitable dissociation site. These two reaction mechanisms occur competitively in the moderate translational energy range. The portion of directly activated dissociation increased with increasing E_i because the number of the dissociation sites where the O_2 molecule can overcome the activation barrier increases. Hodgson et al. have postulated a similar reaction model based on the precise initial sticking probability measured by the King−Wells method at several surface temperatures and incident energies of O_2.[5] Although the initial S value is difficult to precisely estimate using the present data, our research based on the reaction order analysis of Langmuir model agrees well with their postulation.

At $\Theta > 0.5$ ML, oxidation for the thermal O_2 dose and 0.1−0.5 eV HOMB incidence proceeded gradually. During the initial oxidation in a thermal O_2 atmosphere, oxygen surface diffusion is the dominant mechanism for the oxide formation.[34] The thermal O_2 dose and 0.5 eV HOMB incidence had nearly the same S values, implying that oxidation above 0.5 ML for thermal and 0.5 eV O_2 may proceed via the same reaction pathway.

In contrast to the HOMB incidence at $E_i \leq 0.5$ eV, that at $E_i \geq 1$ eV was easily achieved at Θ above 0.5 ML, and Cu_2O was efficiently formed. Figure 3 shows the O-uptake curves for 0.5, 1.0, and 2.3 eV HOMB incidences along the surface normal direction and thermal O_2 exposure. Under a thermal O_2 dose and 0.5 eV HOMB incidence, a huge dosage of $\sim 10^{19}$ molecules·cm^{-2} was required to produce the $c(6 \times 2)$ structure at RT, and further oxidation beyond 0.7 ML proceeded very slowly. These results imply that hyperthermal O_2 with $E_i \geq 1.0$ eV can easily overcome the activation barrier, which should be enhanced by the repulsive interaction due to oxygen adatoms in this coverage region. Consequently, unlike the oxidation of Cu(100)[23] and (111),[25] fitting the uptake curves for hyperthermal O_2 with $E_i \geq 1.0$ using simple Langmuir type kinetics is not feasible.

Figure 4 shows the coverage dependence of the sticking probability calculated from the oxygen uptake curves. The S for thermal O_2 dose and for 0.5 eV HOMB incidence decreased suddenly around $\Theta = 0.5$ ML, and a low probability of 10^{-4} was maintained during further oxidation. In contrast, S for HOMB with $E_i \geq 1.0$ eV at $\Theta > 0.5$ ML was larger than those obtained for the thermal O_2 dose and 0.5 eV HOMB incidence by one or 2 orders of magnitude. Regardless of the large error in S due to the scattered data points in the uptake curves, the difference between S for $E_i \leq 0.5$ eV and for ≥ 1 eV is remarkable. The HOMB with $E_i \geq 1.0$ eV was generated by the high temperature nozzle at $T_n = 1400$ K; thus, both the vibrational and rotational states of oxygen molecules should be excited. Although these internal state excitations affect the difference in S at $\Theta \leq 0.5$ ML, they do not play a significant role during the oxidation process.[35] To verify the possibility of the CIA mechanism where the transfer of the translational energy of impinging O_2 to the O adatom is essential, we measured the O-1s spectra after energetic Ar beams with $E_i \geq 1.5$ eV incidence along the surface normal on Cu(110) saturated by thermal O_2 gas adsorption. Cu_2O formation was clearly induced by 3 eV Ar beam incidence on Cu(100) via a CIA process.[22] In the case of Cu(110), noticeable changes in the line shape of the O-1s peak were not observed (data not shown). Thus, other efficient oxidation mechanisms, which are peculiar to the Cu(110) surface, should be considered.

Figure 5 shows the azimuthal-angle dependence of the sticking probabilities for the 2.3 eV HOMB incidence with a 45° angle of incidence from the surface normal along the [001]

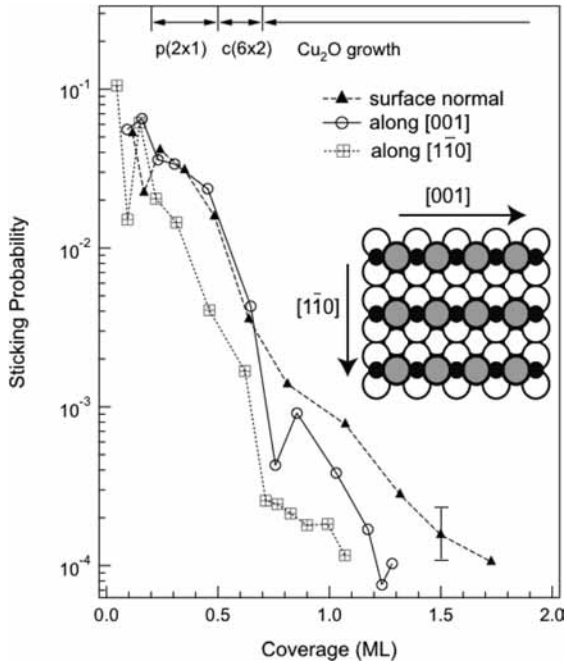

Figure 5. Azimuthal incident angle dependence of the sticking probability (S) on Cu(110) at RT with a schematic drawing of the p(2 × 1)-O structure. Solid triangles, open circles, and open squares are the O-uptake curves for the 2.3 eV HOMB irradiation along the surface normal, along the [001] direction and along the [1$\bar{1}$0] direction, respectively. Angle of the oblique incidence is 45° from the surface normal. Characteristic features of the observed LEED patterns and the O 1s XPS peaks are noted at the top. Inset shows the Cu(110)-O structure where the open circles indicate copper atoms on the Cu(110) surface, and the gray and the black circles indicate copper and oxygen atoms forming the Cu−O row on the surface, respectively. Here S is calculated from the azimuthal-dependent O-uptake curves reported in ref 26.

direction and along [1$\bar{1}$0] direction. The clean Cu(110) surface seen by the O_2 molecules was approximated as flat because the initial value of S is independent of the incident azimuth on a clean surface.[5] In the higher coverage region above 0.2 ML, dissociative adsorption along [001] occurred more efficiently than along [1$\bar{1}$0]; that is, S along [001] was larger than that along [1$\bar{1}$0], suggesting that azimuthal anisotropy of the oxidation efficiency is connected to the appearance of the highly corrugated added row (AR) structure along [001] direction.

Additionally, Figure 5 suggests that the effective oxidation by highly energetic O_2 on Cu(110) may occur around the −Cu−O− rows because the azimuthal dependence of S is intimately connected with the growth of AR. On the basis of the azimuthal-incident-angle dependent sticking probability, we propose the following reaction mechanism. The oxidation on Cu(110) by highly energetic HOMB proceeds via dissociation at troughs of the AR for $\Theta \leq 0.7$ ML, possibly via precursors. The highly energetic O_2 with $E_i \geq 1.0$ eV may access the reactive sites even on the $p(2 \times 1)$ and $c(6 \times 2)$ structures, although the energy barrier for access is enhanced due to the repulsive interaction among the impinging O_2 and Cu−O structure. According to theoretical studies, a 4-fold hollow site on a Cu(110) surface is favorable for O_2 adsorption and subsequent spontaneous dissociation.[20] Such a hollow site on the AR structure is accessible by HOMB along both [001] and surface normal without a shadowing effect. On the other hand, the reactive hollow site is shadowed normal to AR. The corrugation by the AR structure is so large that it inhibits dissociation by the shadowing effect. This scenario is also

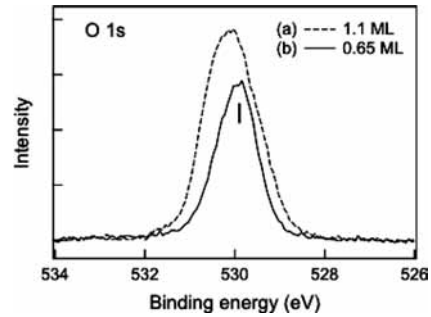

Figure 6. O 1s XPS spectra measured immediately after 2.3 eV HOMB incidence of 1×10^{18} molecules·cm^{-2} with a 45° angle along the [1$\bar{1}$0] direction at RT (a) and after maintaining the sample at UHV of 3×10^{-8} Pa for 2 h at RT (b). Θ in (a) and (b) is 1.1 and 0.65 ML, respectively.

applicable to the oxidation process for $\Theta \geq 0.7$ ML. On the $c(6 \times 2)$ structure, copper atoms alternate between a short bridge site along the [001] in the trough and shadow the reactive site in the trough from the HOMB, even along [001]. This may reduce the sticking probability for the HOMB incidence along [001] for $\Theta \geq 0.7$ ML compared to the normal incidence. (See the solid triangles and open circles for $\Theta \geq 0.7$ ML in Figure 5.)

Figure 6 shows the O 1s XPS spectra measured immediately after 2.3 eV HOMB irradiation with a 45° incident angle from the surface normal along the [1$\bar{1}$0] direction at RT (a) and after being maintained for 2 h in UHV of 3×10^{-8} Pa at RT (b). Cu_2O was easily formed by HOMB at $E_i \geq 1$ eV, and oxygen coverage was achieved above 0.7 ML. For the Cu(110) surface with $\Theta \sim 0.8$ ML produced in O_2 atmosphere, annealing above ~600 K is necessary to reduce Θ.[16] Even at 300 K, excess oxygen atoms on Cu(110) prefer to segregate in the bulk instead of recombining and desorbing into the gas phase.[17] As shown in Figure 6b, on the Cu_2O formed by the 2.3 eV HOMB irradiation, the incorporated O atom above 2/3 ML desorbed even at RT, and the oxygen coverage decreased to 0.65 ML, corresponding to a saturation coverage of the $c(6 \times 2)$-O structure. Hence, Cu_2O formed by the highly energetic O_2 incidence is unstable even at RT, although the copper oxide growing in the O_2 gas atmosphere does not decompose.[16,17]

On a copper surface, Cu_2O islands grow three-dimensionally via oxygen surface diffusion and conversion of copper atoms in a dry oxygen gas atmosphere.[34] In this gradual growth mode, an oxygen adatom diffusing across the surface tends to be trapped at the energetically most favorable site around the oxide island, causing growth. However, the Cu_2O island is highly strained by the large lattice mismatch between bulk Cu and Cu_2O, which limits oxide growth.[36−38] Therefore, to effectively form Cu_2O islands at a higher O-coverage, a higher substrate temperature, which reduces the interfacial strain induced by lattice mismatch, is required. At high temperatures, islands prefer structures with a large average size, which has a deeper penetration but a smaller island density such that at high temperature a thicker oxide island is more energetically favorable than an island with large surface area formed at low temperatrure.[36]

On the other hand, the highly energetic O_2 impinging the trough site may directly dissociate and incorporate into the subsurface to form a Cu_2O structure in the subsurface at RT. In this oxidation mode, the oxygen atoms can adsorb dissociatively and overcome the activation barrier directly at a low substrate temperature. Then lattice mismatch increases the interface strain between the produced Cu_2O island and the surrounding Cu bulk.

HOMB successively induces oxidation before the system has relaxed completely. Thus, for the oxide growth mode using HOMB at low substrate temperature, thin and small oxide islands, which are less stable due to the strain, may be formed with a high number density. On a Cu(110) surface, the CIA process is ineffective, suggesting that the subsurface sites are unstable for trapping oxygen atoms at RT under $\Theta > 0.5$ ML. This result differs from that on closer-packed Cu(100)[22] and Cu(111),[25] and further supports the instability of HOMB-fabricated Cu_2O on Cu(110).

4. Conclusion

We measured the O-1s XPS spectra on a Cu(110) surface and precisely determined the O-uptake curves during HOMB incidence and thermal O_2 dose at RT. The O-uptake curves implied simple Langmuir type kinetics during oxygen adsorption for O_2 with $E_i \leq 0.5$ eV under $\Theta \leq 0.5$ ML. However, the reaction order between one and two, depending on the E_i, suggests that two adsorption mechanisms competitively exist, trapping-mediated adsorption, which is dominant at low E_i, and directly activated adsorption, which becomes important with increasing E_i.

Oxidation at $\Theta > 0.5$ ML proceeds effectively by the energetic O_2 with $E_i \geq 1.0$ eV, but oxidation is gradual during the thermal O_2 dose and the HOMB with $E_i \leq 0.5$ eV incidence. Depending on the azimuthal direction of incident, which is related to the p(2 × 1) added row reconstructed structure, there is a large anisotropy in the sticking probability. The newly opened reaction channel via the troughs of the AR structure by the highly energetic HOMB and the shadowing effect from the reactive hollow site can explain the effective oxidation mechanism by highly energetic O_2 on the Cu(110) surface. Cu_2O formed via the new reaction channel may have metastable structures that cannot be produced in the thermal equilibrium process.

Acknowledgment. All of the experiments were performed using SUREAC2000 in BL23SU at SPring-8. The authors are grateful to Dr. Y. Saitoh and Dr. S. Fujimori for their help operating the monochromatic system at the beamline. M.O. was also supported by MEXT for a Grant-in-Aid for Scientific Research (No. 20350005).

References and Notes

(1) Ohba, T. *Appl. Surf. Sci.* **1995**, *91*, 1.
(2) Musa, A. O.; Akomolafe, T.; Carter, M. J. *Sol. Energy Mater. Sol. Cells* **1998**, *51*, 305.
(3) Sadana, A.; Katzer, J. R. *Ind. Eng. Chem., Fundam.* **1974**, *13*, 127.
(4) Briner, B. G.; Doering, M.; Rust, H.-P.; Bradshaw, A. M. *Phys. Rev. Lett.* **1997**, *78*, 1516.
(5) Hogdson, A.; Lewin, A. K.; Nesbitt, A. *Surf. Sci.* **1993**, *293*, 211.
(6) Pudney, P.; Bowker, M. *Chem. Phys. Lett.* **1990**, *171*, 373.
(7) Wendelken, J. F. *Surf. Sci.* **1981**, *108*, 605.
(8) Mundenar, J. M.; Plummer, E. W.; Sneddon, L. G.; Baddrof, A. P.; Zehner, D. M.; Gruzalski, G. R. *Surf. Sci. Lett.* **1988**, *198*, 216.
(9) Wander, A. *Surf. Sci. Lett.* **1989**, *216*, 247.
(10) Jensen, F.; Besenbacher, F.; Lægsgaard, E.; Stensgaard, I. *Phys. Rev. B* **1990**, *41*, 10233.
(11) Coulman, D. J.; Wintterlin, J.; Behm, R. J.; Ertl, G. *Phys. Rev. Lett.* **1990**, *64*, 1761.
(12) Gruzalskia, G. R.; Zehner, D. M.; Wendelken, J. F. *Surf. Sci. Lett.* **1984**, *147*, L623.
(13) Mundenar, J. M.; Baddorf, A. P.; Plummer, E. W.; Sneddon, L. G.; Didio, R. A.; Zehner, D. M. *Surf. Sci.* **1987**, *188*, 15.
(14) Lawless, K. R.; Gwathmey, A. T. *Acta Metall.* **1956**, *4*, 153.
(15) Feidenhans'l, R.; Stensgaard, I. *Surf. Sci.* **1983**, *133*, 453.
(16) Gruzalskia, G. R.; Zehner, D. M.; Wendelken, J. F. *Surf. Sci.* **1985**, *159*, 353.
(17) Baddorf, A. P.; Wendelken, J. F. *Surf. Sci.* **1991**, *256*, 264.
(18) Ge, J.-Y.; Dai, J.; Zhang, J. Z. H. *J. Phys. Chem.* **1996**, *100*, 11432.
(19) Liem, S. Y.; Kresse, G.; Clarke, J. H. R. *Surf. Sci.* **1998**, *415*, 194.
(20) Liem, S. Y.; Clarke, J. H. R.; Kresse, G. *Surf. Sci.* **2000**, *459*, 104.
(21) Liem, S. Y.; Clarke, J. H. R.; Kresse, G. *Comput. Mater. Sci.* **2000**, *17*, 133.
(22) Okada, M.; Moritani, K.; Goto, S.; Kasai, T.; Yoshigoe, A.; Tearaoka, Y. *J. Chem. Phys.* **2003**, *119*, 6994.
(23) Okada, M.; Moritani, K.; Yoshigoe, A.; Teraoka, Y.; Nakanishi, H.; Dino, W. A.; Kasai, H.; Kasai, T. *Chem. Phys.* **2004**, *301*, 315.
(24) Moritani, K.; Okada, M.; Teraoka, Y.; Yoshigoe, A.; Kasai, T. *J. Phys. Chem. C* **2008**, *112*, 8662.
(25) Moritani, K.; Okada, M.; Sato, S.; Goto, S.; Kasai, T.; Yoshigoe, A.; Teraoka, Y. *J. Vac. Sci. Technol., A* **2004**, *22*, 1625.
(26) Moritani, K.; Okada, M.; Fukuyama, T.; Teraoka, Y.; Yoshigoe, A.; Kasai, T. *Eur. Phys. J. D* **2006**, *38*, 111.
(27) Okada, M.; Vattuone, L.; Moritani, K.; Savio, L.; Teraoka, Y.; Kasai, T.; Rocca, M. *Phys. Rev. B* **2007**, *75*, 233413.
(28) Okada, M.; Vattuone, L.; Gerbi, A.; Savio, L.; Rocca, M.; Moritani, K.; Teraoka, Y.; Kasai, T. *J. Phys. Chem. C* **2007**, *111*, 17340.
(29) Vattuone, L.; Savio, L.; Rocca, M. *Surf. Sci. Rep.* **2008**, *63*, 101.
(30) (a) Yokoya, A.; Sekiguchi, T.; Saitoh, Y.; Okane, T.; Nakatani, T.; Shimada, T.; Kobayashi, H.; Takao, M.; Teraoka, Y.; Hayashi, Y.; Saaki, S.; Miyahara, Y.; Harami, T.; Saaki, T. A. *J. Synchrotron Radiat.* **1998**, *5*, 10. (b) Nakatani, T.; Saitoh, Y.; Teraoka, Y.; Okane, T.; Yokoya, A. *J. Syncrotron Radiat.* **1998**, *5*, 536.
(31) (a) Teraoka, Y.; Yoshigoe, A. *Jpn. J. Appl. Phys.* **1999**, *38* (Suppl. 642), 38–1. (b) Teraoka, Y.; Yoshigoe, A. *Appl. Surf. Sci.* **2001**, *169−170*, 738.
(32) Teraoka, Y.; Yoshigoe, A. *Jpn. J. Appl. Phys.* **2001**, *41*, 4523.
(33) Alatalo, M.; Puisto, A.; Pitkänen, H.; Foster, A. S.; Laasonen, K. *Surf. Sci.* **2006**, *600*, 1574.
(34) Zhou, G.; Yang, J. C. *Surf. Sci.* **2003**, *531*, 359.
(35) Moritani, K.; Tsuda, M.; Teraoka, Y.; Okada, M.; Yoshigoe, A.; Kasai, T.; Kasai, H. *J. Phys. Chem. C* **2007**, *111*, 9961.
(36) Zhou, G.; Yang, J. C. *Appl. Surf. Sci.* **2004**, *222*, 357.
(37) Zhou, G.; Yang, J. C. *Phys. Rev. Lett.* **2002**, *89*, 106101.
(38) Lahtonen, K.; Hirisimäki, M.; Lampimäki, M.; Valden, M. *J. Phys. Chem.* **2008**, *129*, 124703.

JP905564M